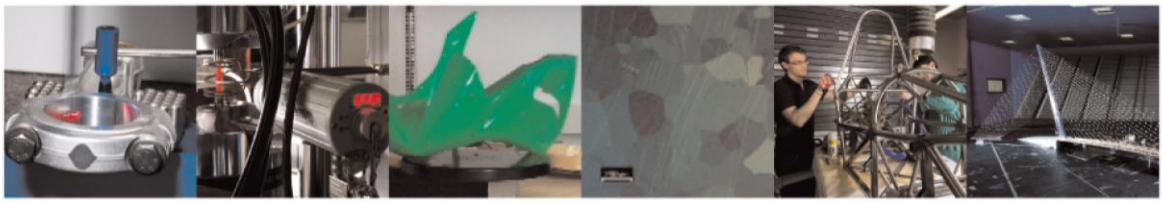

Application of Laser Metal Deposition for a New Model of Assembled Camshaft

Cecchel, Silvia; Ferrario, Davide; Mondini, Claudio; Montani, Marco; Previtali, Barbara

This is a post-peer-review, pre-copyedit version of an article published in JOURNAL OF MATERIALS ENGINEERING AND PERFORMANCE. The final authenticated version is available online at: http://dx.doi.org/10.1007/s11665-019-04504-2

Application of Laser Metal Deposition for a new model of assembled camshaft

Silvia Cecchel,[1, *] Davide Ferrario,[1] Claudio Mondini,[1] Marco Montani[2], Barbara Previtali[2]

[1] Streparava SpA, via Zocco 13, 25030 Adro (Bs), Italy

*E-mail: s.cecchel@streparava.it; Phone: (+39) 030 7459244

[2] Politecnico di Milano, Department of Mechanical Engineering, Via La Masa 1, 20156 Milan, Italy

Keywords: Camshaft, Additive Manufacturing, Laser Metal Deposition (LMD), cladding, testing, hardness, dilution

ABSTRACT

This work introduces the invention of an alternative camshaft manufacturing method aimed at improving the efficiency of the process and providing a more flexible product. The innovation consists in the Laser Metal Deposition (LMD) of a profile on the shaft in order to realise a coupling stretch where the cam is fixed by interference. Alternative profile materials (1.4404 steel and Inconel 625 alloy) are deposited on a 1.0421 steel tube at different laser power levels and powder flow rate. The effect of the process parameters on the deposited profile is investigated initially through the evaluation of indirect quality attributes, such as deposit dimensions, hardness values, and microstructure. Then the coupling force resulting from the press fit test is evaluated. Finally, the best configuration of this new assembled camshaft is tested with a torsion test rig. Performances of the new assembled camshaft are compared with those of traditional products, leading to the validation of this innovative solution. The preliminary feasibility of the LMD application to the production of an assembled camshaft is demonstrated.

1. Introduction

The use of shafts with shaped profiles, for example camshafts, is very widespread in the automotive field for both private and commercial vehicles. In this field, the role of a camshaft is to control the open-and-close intervals of the inlet and exhaust poppet valves through cams movement, which makes camshafts one of the key engine components [1]. Camshaft traditional manufacturing process consists in shaping the whole profile, i.e. shaft and cams together, with different conventional methods, such as casting, forging or machining from a block, just to mention a few, or unconventional, as hydroforming. Cast camshafts for instance are produced by filling with molten grey cast iron a metallic mould (chilled iron casting), thus obtaining a surface virtually free from graphitic carbon [2], composed of a hard ledeburitic structure [3]. Camshafts produced by forging or bar-machining are also used. The former are commonly manufactured on Computer Numerically Controlled (CNC) forging systems with integrated heat treatment, while the latter are CNC-machined directly from steel bars.

The current trend in the design of engine components aims at reducing losses and increasing the efficiency of the powertrain. A way to improve efficiency is to downsize the engine, as smaller engines are more efficient. In this way, the well-known benefits resulting from the weight reduction of vehicles components are also maximised [4-7]. Indeed, numerous studies indicate that a 10%

weight reduction can lower fuel consumption by 6%–7%, if the engine is downsized to maintain constant performance, and by 4%–5%, if the engine is not downsized [8].
In this context, the hydroforming process can be used for manufacturing hollow, and thus lighter, shafts. In camshaft hydroforming, a precursor tube is placed into a die, the ends are sealed with two axial plungers and the tube is filled with hydraulic fluid through one of two punches until it reaches the final camshaft shape [9].
On the other hand, assembled camshafts (made up of two components, that is, cams and shaft) are developed to combine the advantage of a weight reduction with lower costs, higher production efficiency, material optimization, and flexible design and manufacturing [10]. In comparison to cast camshafts, the cost of assembled camshafts is generally cheaper. This is due to lower machining cost and quality assessment costs consequent to the higher quality of components [11]. Usually, assembled camshafts consist of a bar and cams fixed by interference. Just to mention a few, common methods are: i) heat-shrink fit, ii) welding, powder sintering and diffusion bonding, iii) knurling connection, iv) expanding tube joint.
In the heat-shrink fit, the cam to be placed on the shaft is heated up to the right expanded dimension; it is then positioned onto the shaft where it cools down and contracts [12]. Powder metallurgy processes can be used to produce near-net-shape cams that are subsequently diffusion-bonded outside shaft [11, 13].
However, the main, currently used connections are expanding-tube joints and knurling connections, which require more affordable equipment but have a lower assembly precision than heat-deformation joining[10]. In expanding-tube joints, an interference stress is generated between the tube and the cam by the mechanical expansion of the tube with a mandrel [14]. On the other hand, the knurling connection process includes, for each annular cam, three steps: before the housing of the annular cam element is defined, a tube is knurled in correspondence of the housing, and then the annular cam is fixed by interference in the housing [10].
In this context, this work analysed and developed an alternative method for manufacturing an assembled shaft, based on the interference due to an innovative shaped profile. The innovation consists in the Laser Metal Deposition (LMD) of an Additive Manufacturing (AM) helicoid profile on the shaft, in order to obtain a coupling stretch where the cam can be fixed by interference. The new procedure of connection entails press-fitting of each cam through the entire extension of each helicoid profile previously deposited on the tube. The same joining technique could also be applied to other similar applications that require a connection between a cylinder and an annular element. The related benefits are an improvement of process efficiency and the manufacturing of a more flexible product. Indeed, this new technology is less sensitive to dimensional variations of the precursor bar as compared to the other assembling processes previously introduced. Also, the manufacturing method is versatile and can be easily adapted to shafts of different sizes. In addition, this process would be advantageous for both low and high volumes of production. A previous patent [15] pre-introduced this invention while this paper focuses on its in-depth development and characterisation in order to demonstrate that the concept can be implemented in an actual application.
The specific technology used for the AM profile was LMD. LMD is a process in which a laser beam is used to melt an alloy addition onto a substrate [16]. The additive material and a small portion of the substrate are molten by the laser beam. In most cases, powder is used as feedstock material, which is molten onto the workpiece or substrate in a melting pool and therefore forms a strong metallurgical bond [17]. Powders usually have a particle size in the range 45 -150 μm. Gas-atomized spherical particles guarantee the best feeding properties [17].
The prior use of LMD was laser cladding for repairing and surface modification of high-value parts, while recent developments of the process regard micro applications, surface modification and rapid manufacturing. Another trend is towards micro-cladding applications that give higher accuracy and improved precision, resulting in enlarged range of laser-cladding applications [17]. Indeed, the fabricated structures are very accurate, have the highest mechanical strength and have precisely tailored features [18].

It is worth observing that the integrity of the entire assembly is crucial for these key engine components, thus the definition of their most proper configuration is a fundamental principle. The most important issues are the materials, the design and features of the connection and the influence of the AM parameters on the deposit, and tube properties.
In this context, the first purpose of this study has been to analyse and select the most adapted process parameters for the manufacturing of a 1.0421-steel tube and 1.3505-steel cams connected through the innovative AM profile technique. To this aim, the Experiment-Design method was applied to several samples and the results were assessed based on dimensional analysis, hardness and microstructure of the deposit profile.
The selected characteristics were used to manufacture some preliminary prototypes, useful for checking the properties of the invention on actual components. Indeed, also the validation of the concept on a real-case study is fundamental for the success of the invention on critical components such as camshafts. Press-fit behaviour and static torsional strength are the two main indicators for measuring the quality of the connection and assembly. Torsion tests were also performed on both solutions: the innovative LMD camshaft and the traditional camshaft assembled by knurling, in order to calculate and compare the torsional strength.
Finally, the results validated the innovative assembled camshaft and demonstrated the preliminary feasibility of the LMD for the assembly of this particular application.

2. Experimental methods

2.1. Description of structure, materials and requirements

In the new proposed solution, the interference between cam and shaft is obtained thanks to a seven-track helicoid, deposited by LMD, whose single-track height (H_{target}) and average hardness are designed to guarantee not only the interference but also a given torsional strength. Figure 1 shows a sketch of the multi-track deposited over the external surface of the shaft at a given distance *I*.

Figure 1: Seven-track helicoid deposit by LMD on the shaft as interlayer between shaft and cam

In the industrial practice, the shaft surface is covered by a thin layer of oil, that protects the tube from corrosion after the cold-drawn process. Therefore, two conditions of the shaft surface are investigated: *Oil*, as the standard practice requires, and *No-oil*, that means high repeatability of the laser deposition but longer process time and increased difficulty in the process design since a cleaning step with acetone has to be inserted before laser deposition.

The best powder alloys and process parameters for the application are evaluated taking into account some specific requirements, as follows:

1. Deposit hardness as much as possible similar or slightly lower than the average shaft hardness (250±50 HV).
2. Deposit geometrical attributes, in particular height *H* of multi-track helicoid deposit set at a specific average value and confidence interval, hereafter named H_{target}, equal to 300± 100 μm.
3. Lower limit to the deposition speed v_d, 35 mm/s, in order to guarantee a given deposition time for the seven-track helicoid deposit.
4. Torsion strength equal to 400±100 Nm.

Deposition tests are realized on 1.0421-steel tubes, while cams are made of 1.3505 steel. The two steels, very common for assembled camshafts, have the nominal chemical composition given in Table 1.

Table 1: Nominal chemical composition of cam, tube and powders (wt %).

Given the Requirement 1 in section 2.1, two different powders are used for the tests: 1.4404 steel and Inconel 625, hereafter reported as In625. Both alloys were chosen because of their wide availability as LMD spherical powder, their relatively low cost, as well as good laser processability.
Both materials are in form of gas-atomized spherical powder, with a diameter distribution: D10: 45 µm-D90: 125µm.
The chemical compositions of deposit powder materials are reported inTable 1.

According to Figure 1, seven helicoid tracks are deposited on the tubular substrate in two surface conditions, *Oil* or *No-oil*. Fixed process parameters are shown in Table 2. Through a preliminary analysis – which is not reported here for sake of briefness – in order to respect the fixed interaxis value (I=2 mm), the spot diameter on the surface is set at 1.2 mm. On the other hand, the minimum cycle time t_{cycle} is guaranteed by a deposit speed v_d of 35 mm/s (see Requirement 3 in section 2.1).
The deposit height is one of the tighter constraints (see Requirement 2 section 2.1) and depends from the values of laser power and the powder flow rate. Therefore, in order to properly set this parameter a Design Of Experiment (DOE) method composed of two levels of laser power and three levels of powder flow rate (2 times replicated) was used.
The range of variable laser power and powder flow rate is shown in Table 3.

Table 2: Fixed parameters in the experiments.

Table 3: Varied parameters in the experiments.

The connection procedure includes the press-fit of each cam through the entire extension of each helicoid profile previously deposited on the tube at room temperature (as shown in **Errore. L'origine riferimento non è stata trovata.**).

Figure 2: Assembled camshaft connected by interference through LMD deposits.

Two cams, about 60 mm distant each other, are assembled on a tube segment 235 mm long.
Two different tests are performed to confirm the connection design and the deposit height. Initially a press-fit test is carried out followed by a preliminary evaluation of the torsion strength.
In order to find the best joining behaviour, two different configurations of the cam inner profile are examined: i) splined (see **Errore. L'origine riferimento non è stata trovata.**a) ; ii) smooth (see **Errore. L'origine riferimento non è stata trovata.**b). Cams with splined inner profile are usually employed in the assembly of traditional knurling technology and consist of many splines oriented parallel to the shaft axis. The splines are obtained from a surface broaching operation that is very expensive. On the other hand, cams with smooth inner profile, do not require broaching and consequently result in a more affordable component with promising perspectives for the current application. The aim of testing the two cams configurations is to evaluate the opportunity to further simplify the innovative process by using a smooth -shape cam profile.

Figure 3: Cam for press-fit test: a) Splined inner profile; b) smooth inner profile.

All the mechanic tests are performed on oiled tubes with In625 AM profiles deposited at laser power 900 W and with powder flow rate = 60 g/min. This is the deposit capable to fit all the Requirements in section 2.1, according to microstructure and hardness analysis on the cross section reported in the next paragraphs.

Moreover, for sake of comparison few additional tests are performed on out-of-range deposit height (Requirement 2 section 2.1). Indeed, two different deposit heights are considered: a value comprised in the H_{target} range (~350 µm) and a higher one (~550 µm) in order to verify the actual compliance with the requirements.

For a comparison, the final mechanical test is conducted also on segments of camshaft assembled with the traditional knurling technology.

2.2. Experimental setups

2.2.1 LMD system

The LMD system is composed of semi-industrial equipment fit to purpose. The core of the system is a coaxial powder deposition head built in-house at the Department of Mechanical Engineering, Politecnico di Milano. The laser source is a 1 kW multi-mode active fibre laser (YLS-1000, IPG Photonics, Cambridge, MA, USA). Feedstock powder is provided to the process head via an industrial powder feeding system (GTV, Luckenbach, Germany). A six-axis anthropomorphic robot (ABB IRB 2400-10, Zürich, Switzerland) with a rotary table is used as the positioning system.
Before reaching the deposition head, the laser beam is launched into a 400 μm diameter process fibre. The process fibre is connected to a collimator at the processing head inlet. The process head has a collimation lens and a focusing lens, with 100 mm and 200 mm lengths respectively, to the point that the nominal diameter at the focal point is 0.8 mm. The processing head is equipped with two gas channels: powder carrier and shielding gas. The emission wavelength is 1070 nm and the quality factor M^2 20.

2.2.2 Microstructure and hardness tests

Cross-sections of the seven helicoid tracks are obtained by abrasive saw cutting, abrasive paper grinding and cloth polishing with 1-μm diamond paste. Samples are then etched, to reveal the geometry and microstructure with oxalic reagent for 1.4404 steel powder and Murakami reagent for In625 powder, respectively. Metallographic sections were analysed with Optical microscopy (Leitz Ergolux 200 from Leica, Wetzlar, Germany). Geometrical attributes of the deposit profiles are measured on macro images of the cross section via image analysis while Vickers micro-hardness is measured over the cross sections with 100 gf applied load and 15 s dwell time (VMHT 30A from Leica, Wetzlar, Germany).
Figure 4 reports the geometrical attributes of the deposit: H and W are the deposit height and width while H_{HAZ} and W_{HAZ} are the heat-affected zone height and width, respectively. On the other hand, H_D represents the height of the deposit dilution within the substrate, while HV_x and HV_y correspond to the Vickers micro-hardness along axis x and y, respectively. In particular, HV_y is measured in order to evaluate the hardness in both the deposit and the HAZ along the deposition axis, while HV_x provides information about the HAZ entity and extension along a transversal axis to the laser direction.

Figure 4: Geometrical attributes of the deposit: hardness, dilution and microstructure measurements representation.

A Scanning Electron Microscope (SEM, Zeiss Evo 50XVP from Zeiss, Oberkochen, Germany), equipped with an energy-dispersive spectrometer (EDS), is also used to quantify the chemical dilution.

2.2.3 Press-fit test

The press-fit experiments are performed on a hydraulic press composed of an Enerpac RC1010 cylinder equipped with a modular air pump, a FACOM frame, and a 100 kN load cell.

Firstly, both splined and smooth profile cams (see Fig. 4) are pressed by interference on the tube in correspondence of the AM deposit, and then the coupling is disassembled by pressing out the cams from the assembled shaft. The interface surface is visual inspected, because the preservation of the AM deposit is considered a fundamental parameter.

In particular, the maximum press fit load, $L_{max\text{-}in}$, and the maximum disassembling load, $L_{max\text{-}out}$, are measured in order to estimate the joining resistance. At least three measurements are taken, and the average value is considered for each condition.

2.2.4 Preliminary static torsion test

A simplified torsion test is conducted to obtain a preliminary estimate of static torsion strength ($T_{max,ext}$). The test is performed on camshafts having cams pressed in place by interference with the same procedure described above. After the assembly, the tube is clamped while the torsion load is manually applied to the cam with a dynamometric key until the joint failure. The strength at break measured by the key is a first estimation of $T_{max,ext}$. At least three measurements are taken, and the average value is considered for each condition.

It is worth to point out that $T_{max,ext}$ value is considered only for comparison purposes, together with the $L_{max\text{-}in}$ and $L_{max\text{-}out}$ from the press-fit test and the deposit characterization, in order to select the most adequate process parameters and the geometry of the connection. Indeed, the torsion resistance of the joining is more accurately evaluated by means of specific and more rigorous quasi-static torsion tests rig.

2.2.5 Quasi-static torsion test rig

A more accurately evaluation of the joining torsional behaviour is performed with quasi-static torsion tests rig.
The experiments are conducted on the computer-controlled electrohydraulic servo-system MTS test bench with equipment fit to purpose at the Streparava Testing Centre.
In particular, the test bench is composed of: i) MTS 244 hydraulic actuator, ii) Linear Variable Differential Transducer (LVDT), iii) load cell and tools specifically designed and built in-house at Streparava Testing Centre in order to clamp the shaft and apply the torsion load to the cams.
The test is carried out under torsional load starting from the maximum dynamic torque (50 Nm), that is 5% increased at each cycle. The test may take few cycles of loading to produce a failure and ends when an angular displacement of the cam lobe relative to the shaft occurs. The torsion value registered is the camshaft T_{max}. For a comparison, this final test is performed on camshafts joined both with the new AM process and with the reference knurling technology.
At least five measurements are taken, and the average value is considered for each condition.

3. Results and Discussion

3.1 Production and characterisation of deposit on tubes

3.1.1 1.4404 steel powder

Figure 5 shows the overviews of the deposits obtained in 1.4404 steel on a tube with oiled surface. At a visual inspection, 1.4404 steel multi-tracks reveal a regular profile, smooth surface with few sintered particles and no cracks or delamination from the substrate.

Figure 5: Examples of the macro aspect of the LMD deposit on a tube with oiled surface in 1.4404 steel (Laser power 900 W, powder flow rate 60 g/min).

Figure 6 reports an example of a single-track cross section obtained with 1.4404 steel. The deposit has a nail-shaped cross section, it is free of cracks or porosities, and is fully melted to the substrate.

Figure 6: Optical microscopy of LMD track cross-sections for 1.4404 steel powder

Figure 7 shows a high magnification of cross-section in Figure 6. The microstructure reported in Figure 7 reveals three different areas in the substrate: dilution, HAZ, and base material. In the latter, the classical ferrite (light phase) and pearlite (dark phase) microstructures can be noted. The microstructure exhibits a banded structure, that is common in commercial wrought products such as tubes. Martensite microstructure appears in the HAZ for a limited depth of about 0.15 mm.

Figure 7: Optical microscopy of laser tracks cross-sections for 1.4404 steel powder: a) dilution zone, b) heat affected zone, c) base material.

Figure 8 reports the deposit height for 1.4404 steel in the two surface conditions, *Oiled* and *Non-oiled*, as a function of laser power and powder flow rate.
As expected, higher powder flow rate considerably increases the track height due to a major deposited volume per unit length of track [19-21]. Also, with greater laser beam power the deposition heights increase, but less significantly.

As regard the surface condition, non-oiled 1.4404 steel tube significantly satisfies the Requirement 2 in section 2.1 only for the maximum flow rates (i.e. 60 g/min at 700 and 900 W); while oiled, 1.4404 steel tube shows a lower profile height and the target value is not achieved. Therefore, when 1.4404 steel is used, the shaft surface must be cleaned with acetone as in the experiments or with other opportune cleaning substances. This would imply the addition of a further step in the camshaft production cycle. Given this limitation, the best process parameter conditions that are included in the rectangular area in Figure 8 are for both laser power levels, 700 and 900 W, i.e. those with a powder flow rate of 60 g/min. These conditions are further investigated for compliance with requirements.

Figure 8: Deposit height for 1.4404 steel, as a function of laser power, powder flow rate and shaft surface condition (dotted line is the reference average micro-HV value, while rectangular area is HV ± dev.std)

Figure 9 resumes the geometrical attributes, used to quantify the influence of the thermal interaction of the laser beam with the shaft substrate. As expected, dilution and thermal damage depend on the energy released to the substrate, given all the other factors constant.

Figure 9: Geometrical attributes of the deposit in 1.4404 steel (powder flow rate 60 g/min; No-oil surface condition)

An example of the trend of HVy (a) and HVx (b) as a function of the laser power for 1.4404 steel in non-oiled surface condition is illustrated in Figure 10.

Figure 10: Trend of micro-hardness values in 1.4404 steel deposit: a) along HVy direction; b) along Hvx as a function of the laser power (dotted line is the reference average micro-HV value while rectangular area is HV ± dev.std)

A HV micro-hardness of about 450 HV is found in the deposit zone of 1.4404 steel, much higher than the wrought standard level hardness for this alloy (230 HV). This could be related to a carbon increase in the cladding after the deposition due to the interaction of the low carbon (0.016% wt) 1.4404 steel powder with higher carbon (0.19%wt) 1.0421 steel base material (seeTable 1). The higher content in carbon in the fusion zone, combined with the very rapid cooling process, generates a finer microstructure, thus enhancing hardness. This observation is in line with similar findings in the referred literature [20, 22]. Requirement 1, section 2.1, is not met by the 1.4404 powder because of the increase in carbon content due to the rapid dilution between the substrate material and the deposit. Therefore, the 1.4404 powder is unfit for the new LMD camshaft concept because the target deposit height is achievable only with a clean shaft but, in any case, with an excessive deposit micro-hardness.

3.1.2 In625 powder

At a visual inspection, In625 multi-tracks reveal a less regular profile than 1.4404 steel with a rough surface covered by sintered particles, while no cracks or delamination from the substrate are observed (see Figure 11).

Figure 11: Examples of the macro aspect of the LMD deposit on a tube with oiled surface in In625 (Laser power 900 W, powder flow rate 60 g/min).

Figure 12 reports an example of a single-track cross section obtained with In625 powder. The LMD deposit has a nail-shaped cross section with evident sintered powder over the surface. Besides, it is free of cracks or porosities and fully molten on the substrate

Figure 12: Optical microscopy of LMD track cross-sections for In625 powder (laser power 900W, powder flow rate=60 g/min, oil condition)

Figure 13 illustrates the deposit height for In625 in the two surface conditions, *Oil* and *No-oil*, as a function of laser power and powder flow rate.

Figure 13: Deposit height for In625, as a function of laser power, powder flow rate and shaft surface condition (dotted line is the reference average value H_{target} while rectangular area is $H_{target} \pm$ dev.std)

The comparison between In625 and 1.4404 steel clad heights shows a higher value for the former material in both oiled and non-oiled condition. The difference can be related to In625 lower thermal conductivity (thermal conductivity of In625 and 1.4404 steel is 10 and 16.2 W/mK, respectively) that determines a higher amount of molten powder resulting in increased clad heights. The higher efficiency of the alloy with the lowest thermal conductivity (In625) also corresponds to an improved process yield even in the oil surface condition. These considerations explain the difference observed between the two tested materials.

As concern the Requirement 2 in section 2.1, the *oiled* surface condition is not a limit to the deposit height, and indeed the target height is reached. Therefore, both laser power levels, 700 and 900 W, at a powder flow rate of 60 g/min, are valid process parameters leading to a deposit height fully included in the rectangular area of Figure 13. These conditions are further investigated in terms of the other requirements.

Figure 14 summarises the geometrical attributes used to quantify the influence of the thermal interaction of the laser beam with the shaft substrate in the two selected process conditions. As expected, dilution and thermal damage depend on the energy released onto the substrate, which means e.g. laser power given all the other factors constant.

Figure 14: Geometrical attributes of the deposit in In625 (powder flow rate 60 g/min; Oil surface condition)

It can be noticed that the H_D values measured for In625 (~240 μm max) are lower than the 1.4404 steel ones (see Figure 11), as well as the HAZ extension. Thus, these parameters are better for In625, since it is worth noting that, in conventional laser cladding processes, the dilution and HAZ is usually undesirable. Besides this general consideration, a minimum dilution amount is always required to guarantee a fully dense bond with the substrate [19]. This assumption is even more relevant in this particular LMD application, where the deposit has to be firmly bound to the substrate in order to create a steady and reliable connection during the joining by interference. Consequently, within the limited H_D values measured for In625, a higher amount of dilution is more advisable. Starting from this assumption, 900 W laser power guarantees a higher amount of dilution with a slight increase in HAZ extension. In particular, the HAZ extension has to be better evaluated through the hardness profile.

An example of the trend of HVy (a) and HVx (b) as a function of the laser power for In625 is ilustrated in Figure 15.

Figure 15: Trend of micro-hardness values In625 deposit: a) along HVy direction; b) along Hvx as a function of the laser power (dotted line is the reference average value micro-HV while rectangular area is micro-HV ± dev.std)

The micro-hardness values on the deposits meet the Requirement 1 in section 2.1.
The analysis of these graphs confirmed the small difference in HAZ extension between the two conditions, i.e. 700 and 900 W, having similar maximum hardness values that entirely fulfil requirement 1. The HV values, for both the laser powers, are much lower than the 1.4404 steel revealing a better behaviour of In625 also for this requirement.
It can also be noticed that the HV micro-hardness in the fusion zone of In625 is quite higher than the standard value for In625, 200 HV [23], reaching values between 250 and 300 HV for both analysed conditions. The reason could relate to secondary hard particles precipitates. Indeed, one of the effects of Fe in Inconel 625 deposit is to promote the precipitation of intermetallics, which entail a hardness increase [24, 25].
The SEM analysis of the In625 deposit cross section reported in Figure 16 confirmed an iron amount increase in the fusion zone in comparison with the nominal composition of the alloy, due to the dilution with the substrate.

Figure 16: SEM analysis image and results of EDS analysis (wt.%) of In625 clad transverse section sample (laser power 900 W, powder flow rate 60 g/min; Oiled surface condition).

Dilution may be measured in different ways based on both dimensional features of the deposit (H_D) and chemical contamination between the deposit and the substrate (hereafter named η).
Equation 1 [26] was used to determine the chemical dilution ratio (η) of the analysis reported in Figure 16:

$$\eta = \frac{\rho_c(X_{c+s}-X_c)}{\rho_s(X_s-X_{c+s})+\rho_c(X_{c+s}-X_c)} \qquad \text{Equation 1}$$

where ρ_c is the density of molten powders (In625; 8.44×10^{-3}g/mm^3) and ρ_s is the substrate density (1.0421 steel; 7.83×10^{-3}g/mm^3); X_{c+s} and X_s are mean weight percent of Fe in the deposit region (38.37%) and substrate (98.1%) respectively; while X_c the weight percent of Fe in the additive material (3.54%).

The calculation gives a chemical dilution ratio of 39%, similar to the values founded by other works in similar condition [24]. It is worth noting that the condition analysed correspond to the process parameters that give the highest H_D values (laser power 900 W).

After all these analysis, the alloy and process parameter that better fulfil the requirements reported in section 2.1 is In625 with laser power 900 W and flow rate 60 g/min in the oiled surface condition. Indeed, the LMD deposit micro-hardness is aligned with the requirement, while for 1.4404 steel the value was too high. In particular, the hardness analysis suggests a good mix between the added layer and the substrate, similar for 700 and 900 W laser power conditions. Being similar the micro-hardness profile, the choice of the 900 W laser power parameter stands in a foreseen better coherence of the deposit with the substrate, due to a higher H_D value. The selected process parameters guarantee the achievement of the In625 profile target height even in the oiled condition, not possible for the other alloy tested. The avoidance of an additional cleaning station simplifies the process and reduces the overall cycle costs. Furthermore, In625 cross section showed a lower dilution and heat-affected zone than 1.4404 steel. Finally, 1.4404 steel behaves better only in terms of surface aspect, that is a less relevant parameter than the hardness of the deposit and its interaction with the substrate. This aspect was confirmed also by the integrity of the connection between the deposited tube and the smooth-profile cam reported in section 3.2.

3.2 Assembly mechanical properties

Table 4 reports the values of $L_{max\text{-}in}$, $L_{max\text{-}out}$ and T_{max} for press-fiting and disassembling tests on deposit heights corresponding to the target H_{target} (~350 μm) with two cam profiles: splined inner profiles (i) smooth inner profile (ii); compared to literature values [10] referred to knurled assembled camshaft tests coupled with traditional splined cams (iii).

Table 4: Press-fit test and torsion tests results for samples with clad height ~350 μm.

On the other hand, Table 5 reports the values of $L_{max\text{-}in}$, $L_{max\text{-}out}$ and $T_{max,ext}$ for press-fitting and disassembling tests on new AM camshaft having a clad value higher than the target one (~550 μm), connected with splined profile cams. These tests on out-of-range deposit heights, are carried out to verify the adequacy of the most critical requirement in section 2.1 (requirement 1).

Table 5: Press-fit test and torsion tests results for samples with clad height ~550 μm.

Regarding the new AM camshaft with splined cams (Table 5), the maximum deposit height tested determines a relevant removal of the LMD deposit during the press-fitting activity. Consequently, the load registered during the coupling by interference ($L_{max\text{-}in}$), is very high while the disassembling one ($L_{max\text{-}out}$) is lower due to the damage of the interface. Also, the preliminary static torsion strength is higher than the reference value. On the other hand, a lower deposit height (Table 4) preserves the LMD deposit and shows a more homogeneous behaviour during pressing and disassembling. This results in a $L_{max\text{-}in}$ value comparable to $L_{max\text{-}out}$, being both lower than the other configuration tested. $T_{max,ext}$ is aligned to the reference value and to Requirement 4 in section 2.1.

The visual inspection of cam and shaft surfaces confirms these results. An example of the joining aspect after pressing-out the connection between LMD deposit and splined-profile cam is shown in Figure 17. The removal of the LMD deposit attached to the cam teeth is evident in the picture. This is verified for all the analysed splined-profile cams. It is worthwhile to note that the coherence of the connection is a fundamental characteristic especially for engine components, which require clean and reliable structures.

Figure 17: Example of cylindrical splined-profile (a) and smooth-profile (b) cams after disassembling of the connection.

The above considerations lead to the selection of H_{target} for further investigations on the smooth cams coupling.

On the other hand, the visual inspection of connections (Figure 17) reveals that smooth-profile cams present only a slight mechanical wear on the inner profile while preserving the deposit integrity. This has been verified for every joining analysed and lead to the selection of smooth-profile cams for the final connections. In addition, smooth-profile is much easier to be produced than splined one, resulting in a more affordable process.

The configuration with deposit height corresponding to H_{target} and smooth-profile cam was selected for the final investigation with torsion test rig.
The average torsion strengths registered for the assembled camshaft manufactured with the traditional technology and with the new LMD connection were 427 ±49 and 426 ±76 Nm respectively.

The innovative assembled camshaft fulfilled Requirement 4 of section 2.1, with values of T_{max} immediately close to that of components manufactured through the traditional process. These values are also very similar to reference [10] one reported in Table 4.

This final result validates the innovative camshaft assembly method in the tested specific conditions.

4. Conclusions

This work analyses and develops an innovative method for manufacturing an assembled camshaft based on a LMD deposit on the shaft in the locations where cams are fixed by interference.

Firstly, the study aimed at finding the most adequate process parameters and materials for the LMD deposit. The results identified the following best configuration:

- Powder alloy: In625
- Laser power: 900 W
- Flow rate: 60 g/min
- Oiled surface condition

Samples produced with this set of parameters fulfil all the process requirements (hardness, clad height, HAZ extension, process affordability).

The coupling stretch robustness during both assembling and disassembling of the connection was then analysed. The best joining configuration verified is:

- Cams with smooth inner profile,
- Minimum coupling interference.

Finally, the best configuration of this new assembled camshaft was validated with a torsion test rig representative of the operating condition of the joining during its lifetime. The same test was also performed on the traditionally-manufactured piece for comparison purposes. The torsion strengths measured were:

- 426±76 Nm for the new assembled camshaft.
- 427±49 Nm for the traditional process.

Please remind that the torsion strength value required for the application was 300 Nm. Thus, the new assembled camshaft successfully passed the test, with results aligned with the traditional manufacturing process. This outcome validates the innovative assembly procedure for camshafts with the selected materials and process parameters in the tested specific conditions.

In conclusion, the present research shows a new method for manufacturing assembled camshafts, where cam and shaft dimensions and materials may vary and could be changed, since LMD-deposit is very flexible technique, adaptive and tailored. Moreover, the shaft surface condition (oiled) and cam inner profile (smooth) are two pre-requisites for an efficient manufacturing cycle with a reduced and simplified sequence of steps (no need for cleaning and broaching), providing for a more flexible production method. The selected assembly features could also be extended to other similar applications that require a connection between a cylinder and an annular element. The advantages would be similar to those already introduced for the current case study.

Acknowledgements

The authors are grateful for the support given in the execution of test rigs by Streparava staff, particularly to Engineer Luca Cordioli and Engineer Fabio Cibolini.

References

1. Ping L., Fengjun L., Anke C., Bokang W., Fracture analysis of chilled cast iron camshaft, (2009), China Foundry, 6:104-108.
2. Kumruoglu L.C., Mechanical and microstructure properties of chilled cast iron camshaft: Experimental and computer aided evaluation (2009) Materials and Design 30: 927–938.

3. Yang Y., Rosochowski A., Wangb X., Jiang Y., Mechanism of "black line" formation in chilled cast iron camshafts, (2004) Journal of Materials Processing Technology 145: 264–267.
4. Cecchel S., Ferrario D., Panvini A., Cornacchia G., Lightweight of a cross beam for commercial vehicles: development, testing and validation; Materials and Design, 2018, 149, p. 122–134, https://doi.org/10.1016/j.matdes.2018.04.021
5. Helms H., Lambrecht U., The potential contribution of light-weighting to reduce transport energy consumption. (2007) Int J Life Cycle Assess, 12:58–64.
6. Dioni D., Cecchel S., Cornacchia G., Faccoli M., Panvini A.; Effects of artificial aging conditions on mechanical properties of gravity cast B356 aluminum alloy, Transactions of Nonferrous Metals Society of China, 2015, vol. 25, issue 4, pp. 1035-1042
7. Cecchel S., Cornacchia G., Gelfi M.; Corrosion behavior of primary and secondary AlSi High Pressure Die Casting alloys, Materials and corrosion, 2017, vol. 68, issue 9, pp. 961-969
8. Isenstadt A. et al., Lightweighting technology development and trends in U.S. passenger vehicles, (2016), International council on clean transportation, https://www.theicct.org/sites/default/files/publications/ICCT_PVtech_lightweighting_wp2016-25.pdf
9. Zhang Q., Wu C., Zhao S. Less loading tube-hydroforming technology on eccentric shaft part by using movable die, (2012), Mater Trans 53(5):820–825, https://doi.org/10.2320/matertrans.MF201121
10. Zhang P., Kou S., Lin B., Wang Y., Optimization for radial knurling connection process of assembled camshaft using response surface method, (2015) Int J Adv Manuf Technol, 77:653–661, https://doi.org/10.1007/s00170-014-6486-z.
11. Yamagata H., The science and technology of materials in automotive engines, Woodhead Publishing limited, (2005), p. 128
12. Quaas R., Method and assembly system for manufacturing an assembled camshaft, (2004), Patent number US20060005385 A1
13. Kim Y.K., Park Y.S., Song J.H., Han D.K., Kim H.Y., Method of Manufacturing Camshaft, (2011), Patent number US20140223736 A1
14. Blanchard P, Nigarura S, Trasorras JRL, Wordsworth R (2000) Assembled camshaft with sintered cam
15. Mondini C., Ferrario D., (2016), Method for manufacturing a shaft with shaped profile, Patent number WO2016181363 A1
16. Torims T., The Application of Laser Cladding to Mechanical Component Repair, Renovation and Regeneration, Chapter 32 in DAAAM International Scientific Book 2013, pp. 587-608, B. Katalinic & Z. Tekic (Eds.), Published by DAAAM International, Vienna, Austria, (2013) DOI: 10.2507/daaam.scibook.2013.32The application of laser cladding to the mechanical component repair, renovation and regeneration,
17. Kaierle S., Barroi A., Noelke C., Hermsdorf J., Overmeyer L., Haferkamp H., Review on Laser Deposition Welding: From Micro to Macro, Physics Procedia 39 (2012) 336 – 345
18. Nowotny S., Current use of laser technology for build-up welding applications, in Surface Engineering, 27 (4), 2011, pp. 231-233
19. Abioye T.E., Folkes J., Clare A.T., A parametric study of Inconel 625 wire laser deposition, Journal of Materials Processing Technology 213 (2013) 2145– 2151, http://dx.doi.org/10.1016/j.jmatprotec.2013.06.007
20. Caiazzo F., Alfieri V., Laser-Aided directed energy deposition of steel powder over flat surfaces and edges, Materials 2018, 11, 435, 1-15, doi:10.3390/ma11030435
21. He X., Mazumder J., Transport phenomena during direct metal deposition, Journal of Applied Physics 101, 053113 (2007); doi: 10.1063/1.2710780
22. Zhang K., Wang S., Liu W., Shang X., Characterization of stainless steel parts by Laser Metal Deposition Shaping, Materials and Design 55 (2014) 104–119, http://dx.doi.org/10.1016/j.matdes.2013.09.006

23. https://www.gtv-mbh.com/cms/upload/downloads/en/Cladding_and_Hardfacing_Powders_2014.pdf
24. Abioye T. E., Farayibi P. K., Clare A. T. (2017) A comparative study of Inconel 625 laser cladding by wire and powder feedstock, Materials and Manufacturing Processes, 32:14, 1653-1659, DOI: 10.1080/10426914.2017.1317787
25. Li, G.; Huang, J.; Wu, Y. An investigation on microstructure and properties of dissimilar welded Inconel 625 and SUS 304 using high power CO2 laser. International Journal of Advanced Manufacturing Technology 2015, 76 (5), 1203–1214.
26. Toyserkani, E.; Khajepour, A.; Corbin, S. Laser Cladding, CRC Press:Boca Raton, FL, 2005

Figures

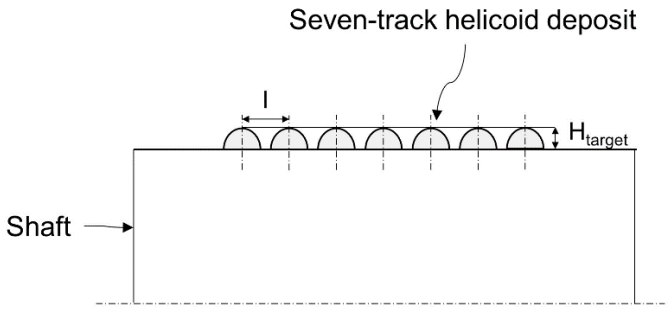

Figure 1: Seven-track helicoid deposit by LMD on the shaft as an interlayer between shaft and cam

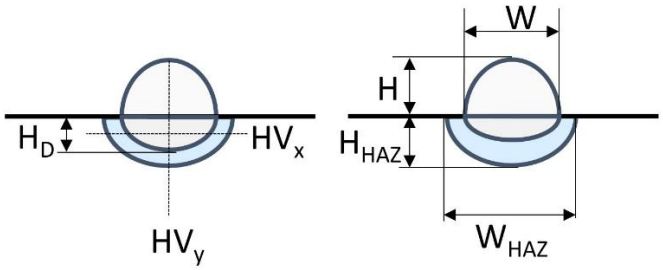

Figure 2: Geometrical attributes of the deposit: representation of hardness, dilution, and microstructure measurements.

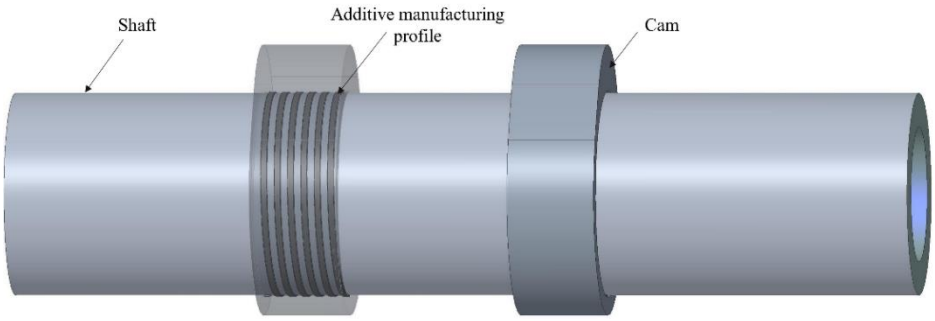

Figure 3: Assembled camshaft connected by interference through LMD deposits.

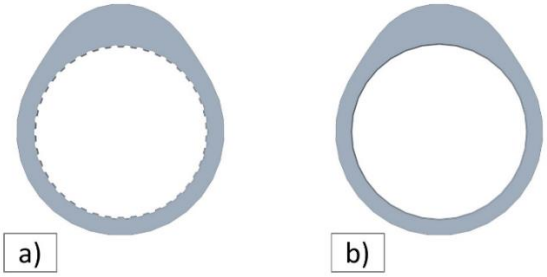

Figure 4: Cam for press-fit test: a) Splined inner profile; b) smooth inner profile.

Figure 5: Examples of the macro aspect of the LMD deposit on a tube with oiled surface in 1.4404 Steel (Laser power 900 W, powder flow rate 60 g/min).

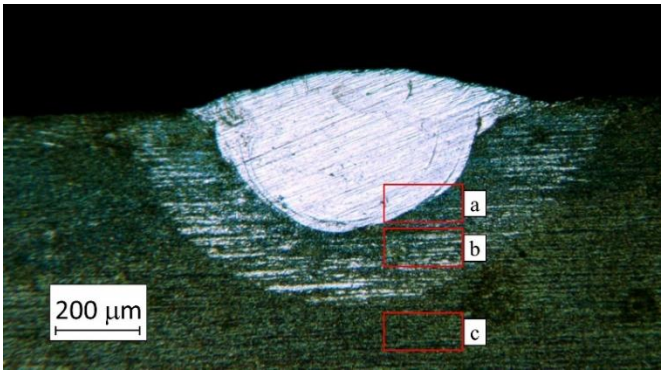

Figure 6: Optical microscopy of LMD track cross-sections for 1.4404 steel powder

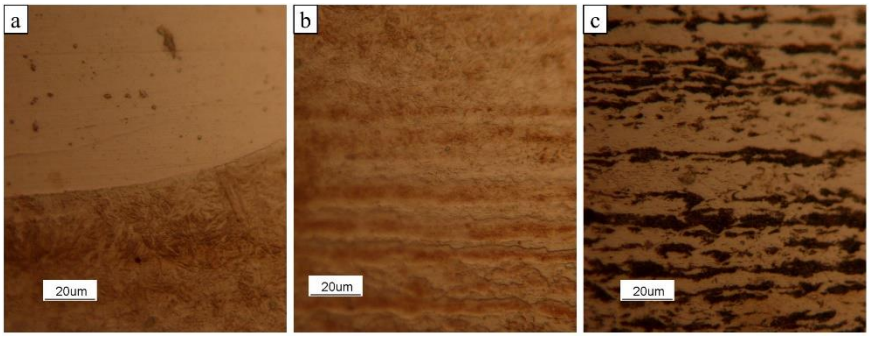

Figure 7: Optical microscopy of laser tracks cross-sections for 1.4404 steel powder: a) dilution zone, b) heat affected zone, c) base material.

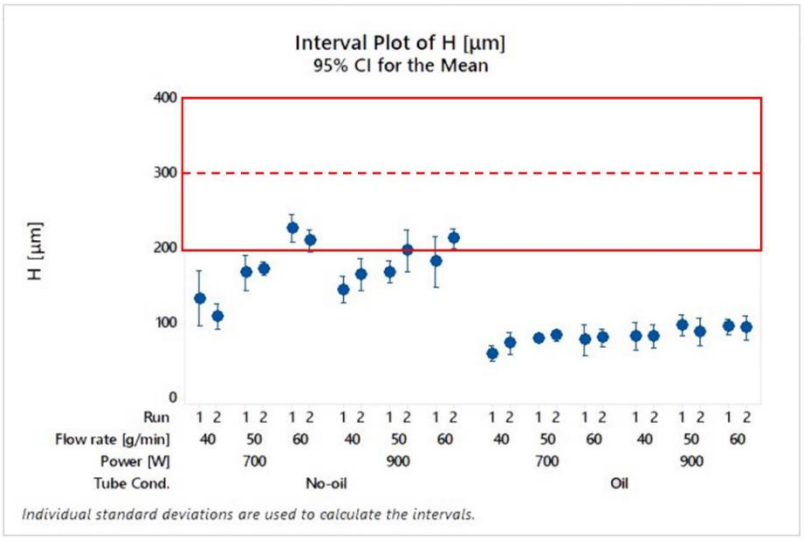

Figure 8: Deposit height for 1.4404 steel, as a function of laser power, powder flow rate and shaft surface condition (dotted line is the reference average H_{target} value, while the rectangular area is $H_{target} \pm$ dev.std)

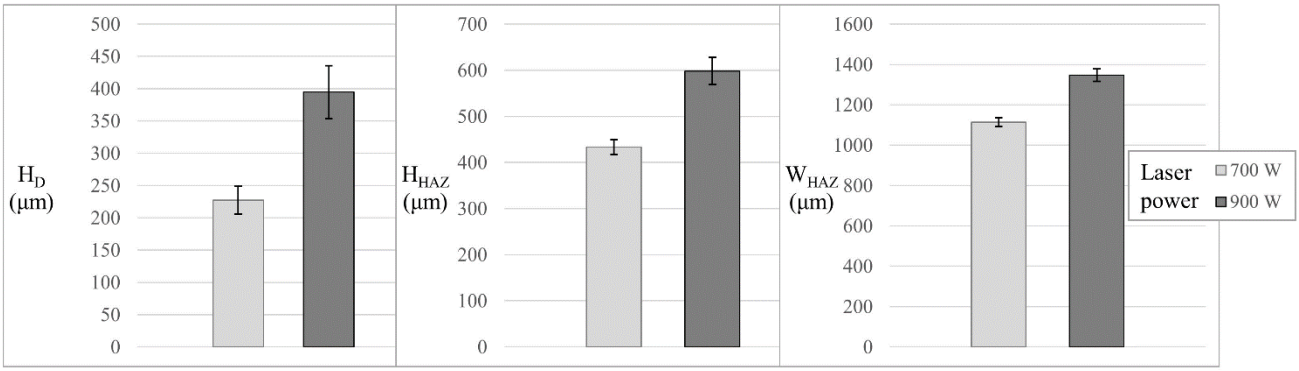

Figure 9: Geometrical attributes of the deposit in 1.4404 steel (powder flow rate 60 g/min; No-oil surface condition)

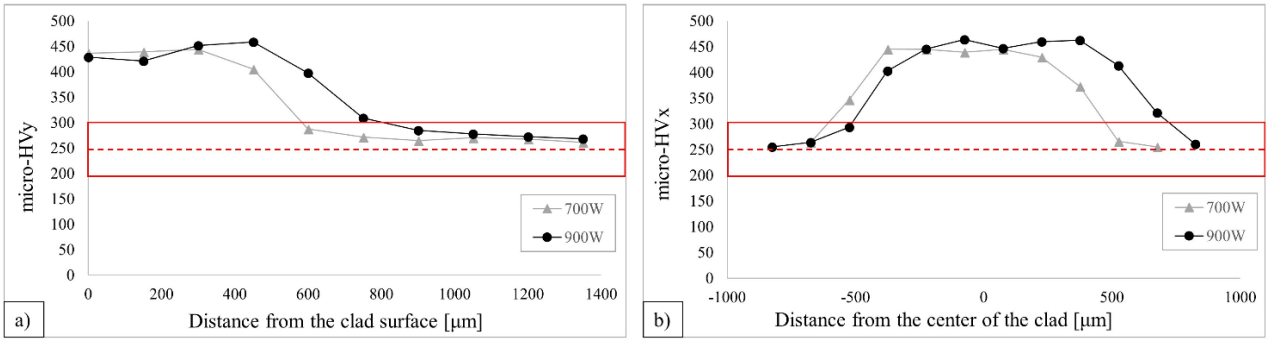

Figure 10: Trend of micro-hardness values in 1.4404 steel deposit: a) along HVy direction; b) along Hvx as a function of the laser power (dotted line is the reference average micro-HV value while rectangular area is HV ±dev.std)

Figure 11: Examples of the macro aspect of the LMD deposit on a tube with oiled surface in In625 (Laser power 900 W, powder flow rate 60 g/min).

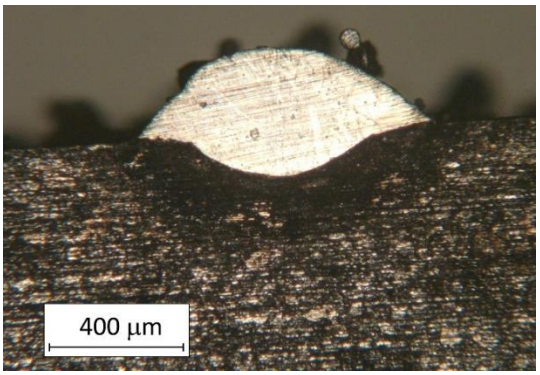

Figure 12: Optical microscopy of LMD track cross-sections for In625 powder (laser power 900W, powder flow rate=60 g/min, oil condition)

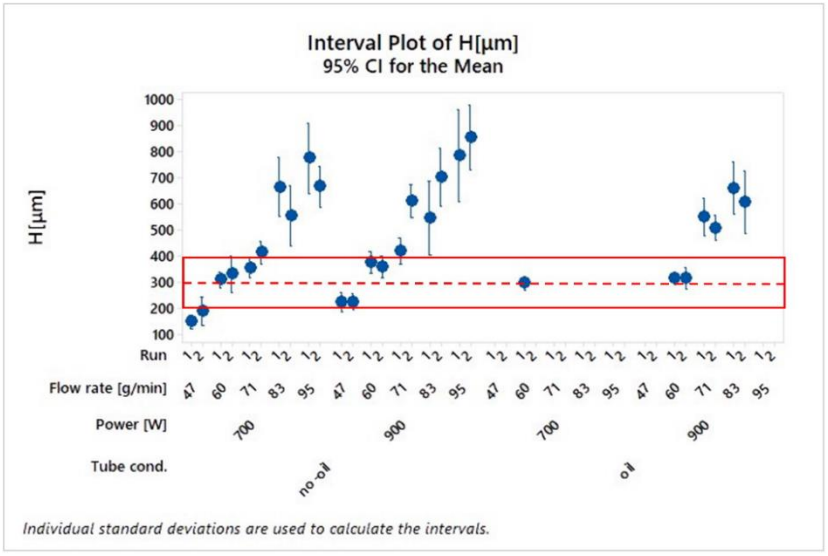

Figure 13: Deposit height for In625, as a function of laser power, powder flow rate and shaft surface condition (dotted line is the reference average value H_{target} while rectangular area is H_{target} ±dev.std)

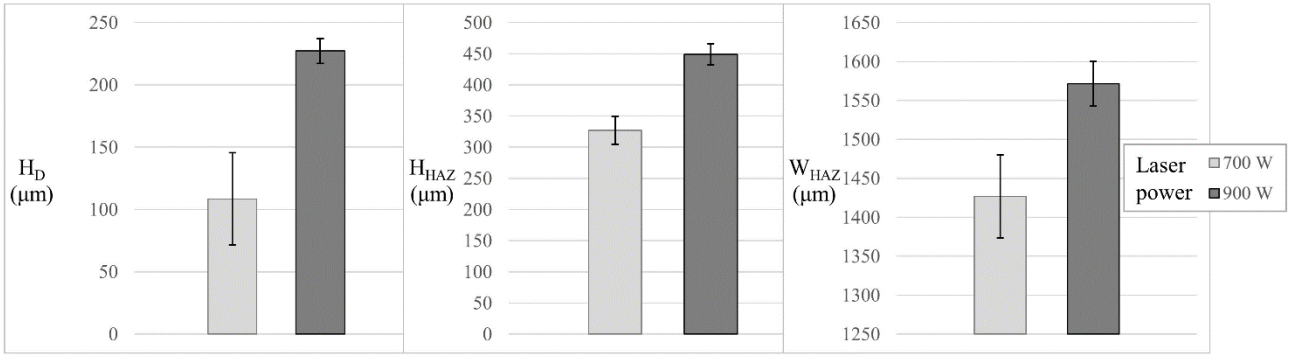

Figure 14: Geometrical attributes of the deposit in In625 (powder flow rate 60 g/min; Oiled surface condition)

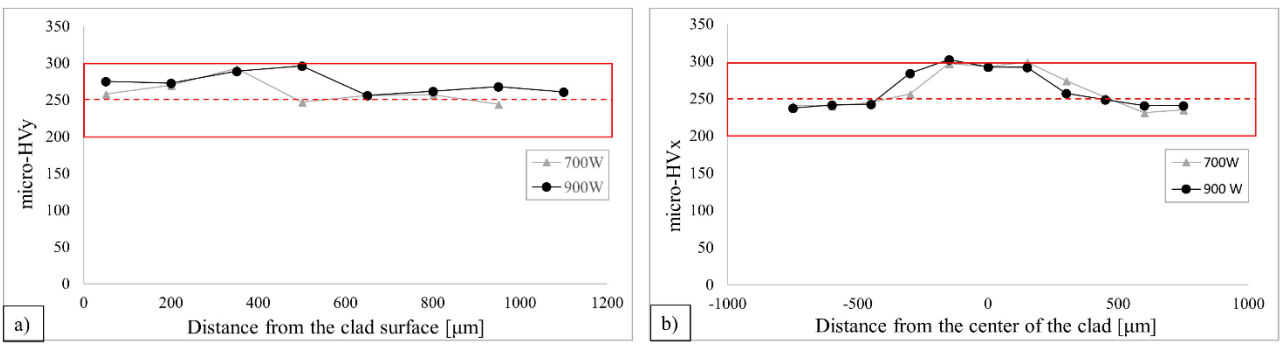

Figure 15: Trend of micro-hardness values In625 deposit: a) along HVy direction; b) along Hvx as a function of the laser power (dotted line is the reference average value for micro-HV, while rectangular area is micro-HV ± dev.std)

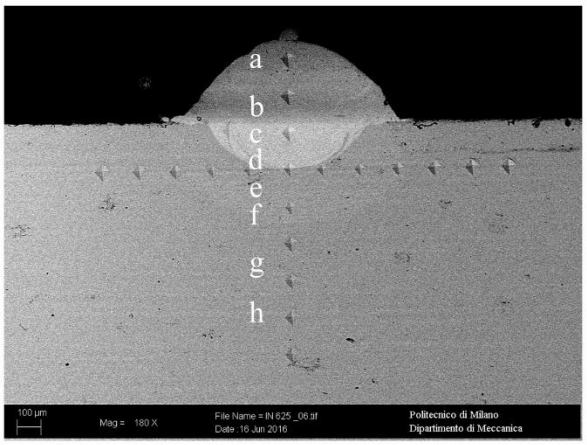

EDS Analysis (wt.%)					
Element	Fe	Ni	Cr	Mo	Mn
a	31.93	41.46	16.46	6.36	0.34
b	36.69	40.95	15.33	5.66	0.6
c	39.23	40.05	14.36	5.61	0.6
d	45.62	35.09	13.2	4.91	0.79
e	97.31	0.25	0.02	0.15	1.99
f	97.68	0.32	0.07	0.21	1.35
g	97.84	0	0.04	0	1.78
h	97.26	0.42	0.21	0.45	1.32
Nominal composition (wt.%)					
In 625	3.54	58.4	21.84	8.96	/
steel 1.0421	98.1	/	/	/	1.41

Figure 16: SEM analysis image and results of EDS analysis (wt %) of In625 clad transverse section sample (laser power 900 W, powder flow rate 60 g/min; Oiled surface condition).

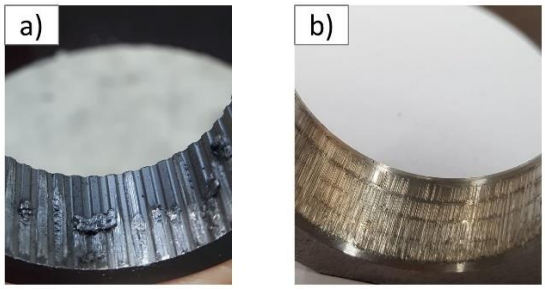

Figure 17: Example of cylindrical splined-profile (a) and smooth-profile (b) cams after disassembling of the connection.

Tables

Table 1: Nominal chemical composition of cam, tube and powders (wt %).

Part	Material	Fe	C	Si	Mn	P	S	Cr	Mo	Ni	Nb	Al
Cam	1.3505	Base	1	0.25	0.35	<0.025	<0.015	1.4	<0.1	/	/	<0.05
Tube	1.0421	Base	0.19	0.18	1.41	0.01	0.003	/	/	/	/	0.03
Powder	1.4404	Base	0.016	0.3	1.4	0.015	0.01	17.77	2.59	11.16	/	/
Powder	In625	3.54	0.011	0.14	0.07	0.01	0.01	21.84	8.96	Base	3.71	/

Table 2: Fixed parameters in the experiments.

Fixed parameters	**Value**
Track interaxis *I*	2 mm
Shielding gas	N_2 at 6 bar
Carrier gas	N_2 at 6 bar
Deposition speed	35 mm/s
Spot diameter	1.2 mm

Table 3: Varied parameters in the experiments.

Varied parameters	**Levels**	
Powder	1.4404	In625
Surface condition.	Oiled	Non-oiled
Laser power	700 W	900 W
Powder flow rate	From 40 to 95 g/min	

Table 4: Press-fit test and torsion test results for samples with clad height ~350 µm.

	Press-fit max load $L_{max\text{-}in}$ (N)	Disassembling max load $L_{max\text{-}out}$ (N)	Torsion strength $T_{max,ext}$ (Nm)
New AM camshaft – with splined cam profile	25210 ± 4255	23867 ± 8787	405 ± 31
New AM camshaft – with smooth cam profile	22030 ± 2503	17755 ± 2581	394 ± 42
Knurled assembled camshaft with splined cam profile [10]	14584		445

Table 5: Press-fit test and torsion test results for samples with clad height ~550 µm.

	Press-fit max load $L_{max\text{-}in}$ (N)	Disassembling max load $L_{max\text{-}out}$ (N)	Torsion strength $T_{max,ext}$ (Nm)
New AM camshaft – with splined cam profile.	51740 ± 5586	31105 ± 2651	648 ± 68